Research Paper

Sulfated polysaccharide of *Sepiella maindroni* ink targets Akt and overcomes resistance to the FGFR inhibitor AZD4547 in bladder cancer

Liping Shan[1], Wei Liu[2], Yunhong Zhan[1]

[1]Department of Urology, Shengjing Hospital, China Medical University, Shenyang, Liaoning 110004, China
[2]Emergency Department, First Hospital of China Medical University, Shenyang, Liaoning, China

Correspondence to: Yunhong Zhan; **email:** yunhongzhan_sj@163.com
Keywords: AZD4547, sulfated polysaccharide of *Sepiella maindroni* ink, bladder cancer, FGFR therapy resistance, xenograft
Received: July 13, 2019 **Accepted:** September 9, 2019 **Published:** September 23, 2019

ABSTRACT

Rapid appearance of resistance to fibroblast growth factor receptor (FGFR) inhibitors hampers targeted regimens in bladder cancer. In the present study, we evaluated whether SIP-SII, a sulphated derivative of the polysaccharide in *Sepiella maindroni* (spineless cuttlefish) ink used in traditional Chinese medicine, could attenuate resistance to FGFR inhibition in bladder cancer cells. In vitro assays indicated that SIP-SII reduced cell viability and migration, restricted cell cycle progression, and increased apoptosis in parallel with decreased AKT phosphorylation and downregulation of CDK4, MMP2, and Bcl-2 in RT112 and JMSU1 cells. Synergistic effects on cell viability were observed when SIP-SII was combined with the small-molecule FGFR inhibitor AZD4547. Specific Akt targeting by SIP-SII was suggested by the fact that neither Akt knockdown nor the selective PI3K inhibitor BKM120 enhanced the inhibitory effects of SIP-II, while expression of a constitutively active Akt mutant rescued SIP-SII effects. Furthermore, subcutaneous transplantation of RT112 xenografts confirmed the superiority and tolerability of combined SIP-SII and AZD4547 administration over monotherapy regimens. The present study thus provides pre-clinical evidence of the ability of SIP-SII to improve FGFR-targeted therapies for bladder cancer by inhibiting Akt.

INTRODUCTION

Bladder cancer is one of the most common cancers worldwide with an estimated 549,393 new cases and 199,922 deaths reported yearly [1]. Men are 4 times more likely than women to be diagnosed with the disease. The general 5-year survival rate for patients with bladder cancer is approximately 77%; however, this rate is reduced to 35% after local dissemination and/or regional lymph node metastasis, and to 5% when distant metastasis develops. In recent years multiple signaling pathways involved in bladder cancer progression have been identified as druggable targets. These include the PI3K/Akt/mTOR pathway, the RTK/RAS/MAPK pathway, and the JAK/STAT pathway [2]. The first targeted therapy for metastatic bladder cancer, the pan-FGFR inhibitor erdafitinib, has recently received FDA approval. Other drugs under current investigation to treat recurrent or refractory bladder cancer include the pan-FGFR inhibitors BGJ398 [3] and AZD4547 [4], aimed at tumors with *FGFR3* mutation or fusion, and the mTOR inhibitor everolimus for refractory bladder carcinoma [5]. A common issue with targeted therapies is intrinsic or acquired resistance of cancer cells. AKT hyperactivation, MET overexpression, *BRAF* fusion, and activation of canonical MAPK-ERK signaling have been implicated in resistance to FGFR inhibitors [6–9]. Therefore, discovery and evaluation of potential compounds that can reverse FGFR inhibitor resistance is critical for improving targeted regimens.

Cephalopod ink has long been used as a traditional medicine in both Eastern (China) and ancient Western cultures [10]. SIP-SII is a sulfated polysaccharide in ink from *Sepiella maindroni* (spineless cuttlefish) which exhibits wide therapeutic potential based on its

anti-tumor, anti-inflammatory, and immunomodulatory activities [11, 12]. Recently, SIP-SII was shown to decrease pulmonary metastasis in a mouse melanoma model by inhibiting ICAM-1-mediated cell adhesion and bFGF-induced angiogenesis [13]. On the other hand, Jiang et al. reported that SIP-SII suppressed cell migration and invasion by targeting the EGFR/PI3K/MMP2 and EGFR/MEK/MMP2 axes in human epidermoid carcinoma KB cells [14]. The same investigators showed that SIP-SII binds to plasma membrane EGFR in ovarian cancer SKOV3 cells, hampering its activation and leading to downregulation of EGFR-mediated p38/MAPK and PI3K/Akt/mTOR cascades [15]. Although a number of studies provided a rationale for the use of SIP-SII as an anticancer agent and a potential therapy to overcome FGFR inhibitor resistance, its pharmacological actions on bladder cancer remain unexplored. In the present study, therefore, we used in vitro and in vivo experiments to explore the potential of SIP-SII to overcome resistance to the FGFR inhibitor AZD4547 in bladder cancer cells carrying active *FGFR* and hyperactive *AKT* mutations.

RESULTS

SIP-SII impairs proliferation and migration and attenuates Akt signaling in bladder cancer cells

To assess the effects of SIP-SII on bladder cancer cell viability, dose-response experiments were performed on RT112 and JMSU1 cells using the MTT assay. Viability was reduced by approximately 50% when RT112 and JMSU1 cells were treated with 6.73 μM and 7.39 μM SIP-SII, respectively (Figure 1A). Hence, IC_{50} concentrations of 2.5 μM and 5 μM were respectively selected to verify SIP-SII's inhibitory effects on cell growth. For the FGFR inhibitor AZD4547, IC_{50} values of 1.25 μM and 1.28 μM were estimated for RT112 and JMSU1 cells, respectively (Figure 1A). Time-course viability experiments were further conducted on RT112 and JMSU1 cells exposed to different concentrations of SIP-SII for 12, 24, 36, or 48 h. As shown in Figure 1B, SIP-SII suppressed cell growth in a dose- and time-dependent manner.

The transwell migration assay was next performed to determine the effects of SIP-SII on cell migration. After incubation with SIP-SII for 24 h, the number of migrating RT112 cells decreased significantly compared to the control group (Figure 1C). Similar results were observed in JMSU1 cells (Figure 1D). Western blotting analysis was further used to detect the expression of total Akt, phospho-Akt, CDK4, Bcl-2, and MMP2. As shown in Figure 1E, after exposure to SIP-SII, the levels of phospho-Akt, CDK4, Bcl-2, and MMP2 declined in a dose-dependent manner, while total Akt showed little variation. Densitometric gel analyses confirmed these results (Supplementary Figure 1A). These data showed that SIP-SII inhibits bladder cancer cell proliferation and migration, while decreasing Akt activation and downstream signaling.

SIP-SII hampers proliferation and migration of bladder cancer cells in an Akt-dependent manner

Previous studies reported that SIP-SII exhibited multiple anti-tumor effects such as suppression of EGFR, FGF, and intercellular adhesion molecule (ICAM)-mediated pathways in ovarian cancer cells and epidermoid carcinoma cells [13] [15]. To verify that Akt inhibition mediates the inhibitory effects of SIP-SII on bladder cancer cells, Akt-targeted siRNAs (si-Akt) were introduced into RT112 and JMSU1 cells. The silencing efficiency of si-Akt was verified by western blotting (data not shown). Cells were treated with control siRNA, 5μM SIP-SII, or the combination of SIP-SII and si-Akt, and MTT and transwell assays were performed 24 h later. SIP-SII alone and in combination with si-Akt repressed cell viability relative to the control group. However, dual treatment did not amplify the inhibition induced by SIP-SII alone, both on cell growth (Figure 2A) or cell migration (Figure 2B and 2C). Western blotting was further performed to determine the activation of Akt and the expression of effector molecules. As shown in Figure 2D and 2E, the decrease in phospho-Akt expression was identical in SIP-SII-treated cells, either when applied alone or in combination with si-Akt, whereas total Akt expression fell significantly only in the latter. Three independent experiments (Supplementary Figure 1B) showed that CDK4 and MMP2 decreased by 16%, Bcl-2 decreased by 25%, phospho-AKT was reduced by 70%, and total AKT expression declined 75% in the combination group. These results indicated that SIP-SII suppressed cell growth and migration by inhibiting Akt activation.

Akt overexpression reverses SIP-SII effects on bladder cancer cells

To further verify that the inhibitory effects of SIP-SII on bladder cancer cell growth and migration relied on inactivation of Akt, a constitutively active Akt mutant, Akt T308D S473D (Akt DD), was introduced into RT112 and JMSU1 cells. Transfected cells were then treated with 5 μM SIP-SII for 24 h, and the MTT assay was performed to assess cell viability. As shown in Figure 3A, Akt DD completely reversed SIP-SII-induced inhibition of cell viability. Moreover, Akt DD expression also attenuated the inhibition of cell migration elicited by SIP-SII (Figure 3B and 3C). Akt DD transfection efficiency was confirmed by western blotting (Figure 3D and 3E). After transfection, the expression of CDK4,

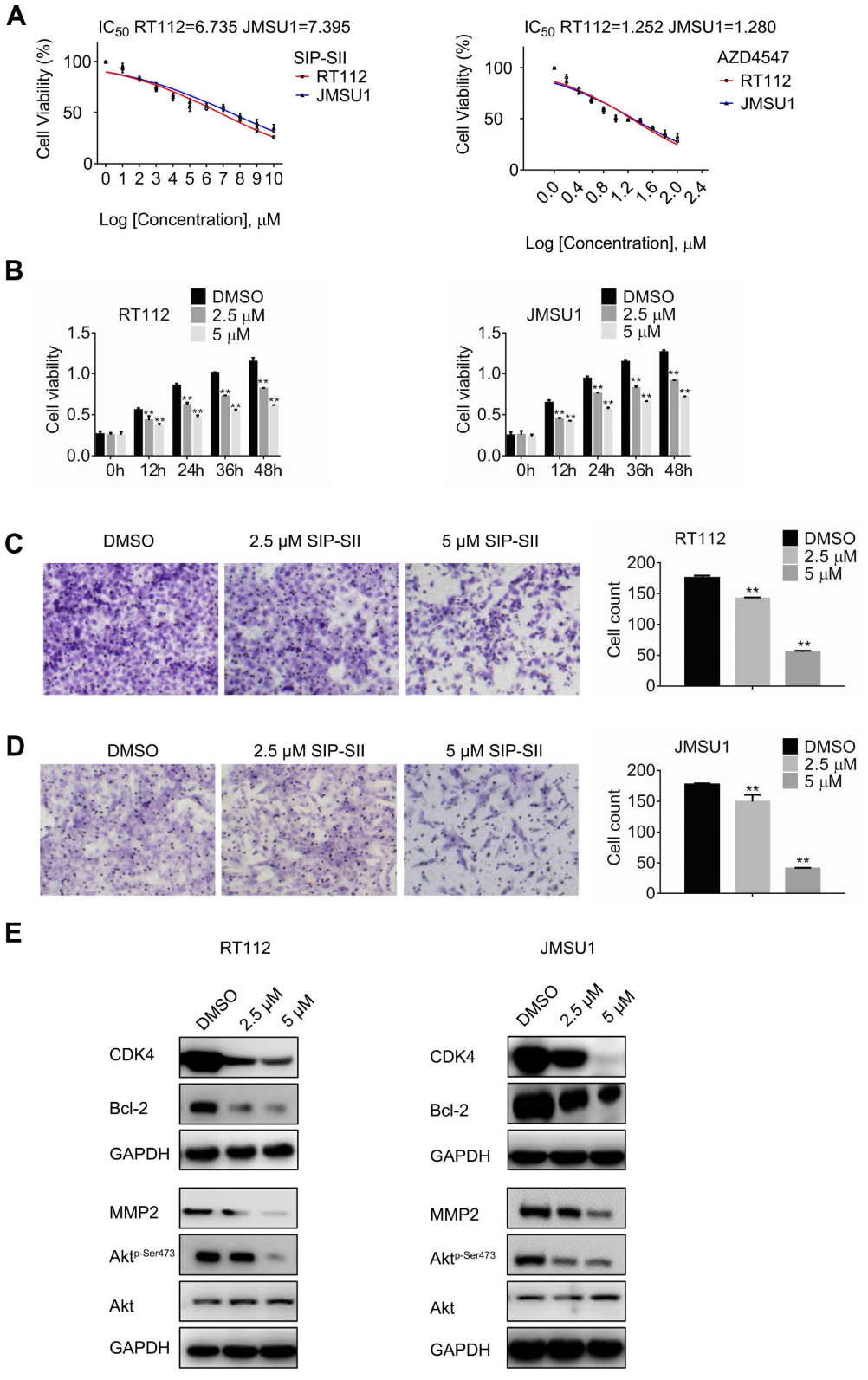

Figure 1. SIP-SII impairs proliferation and migration and attenuates Akt signaling in bladder cancer cells. (**A**) Half-maximum inhibitory concentration (IC_{50}) of test drugs evaluated through the MTT viability assay. (**B**) Cell viability (MTT) assay results for RT112 and JMSU1 cells treated respectively with 2.5 μM or 5μM SIP-SII for the indicated time-points. Cell migration assay results for RT112 cells (**C**) and JMSU1 cells (**D**) treated respectively with 2.5 μM or 5.0 μM SIP-SII for 24 h. Representative images at 200x magnification. Data are mean ± SD (error bars) of three experiments performed in triplicate. **P < 0.01 vs. DMSO (control); n = 3. (**E**) Western blot analysis of total Akt, phospho-Akt, CDK4, Bcl-2, and MMP2 24 h post-exposure to SIP-SII (RT112: 2.5 μM; JMSU1: 5.0 μM).

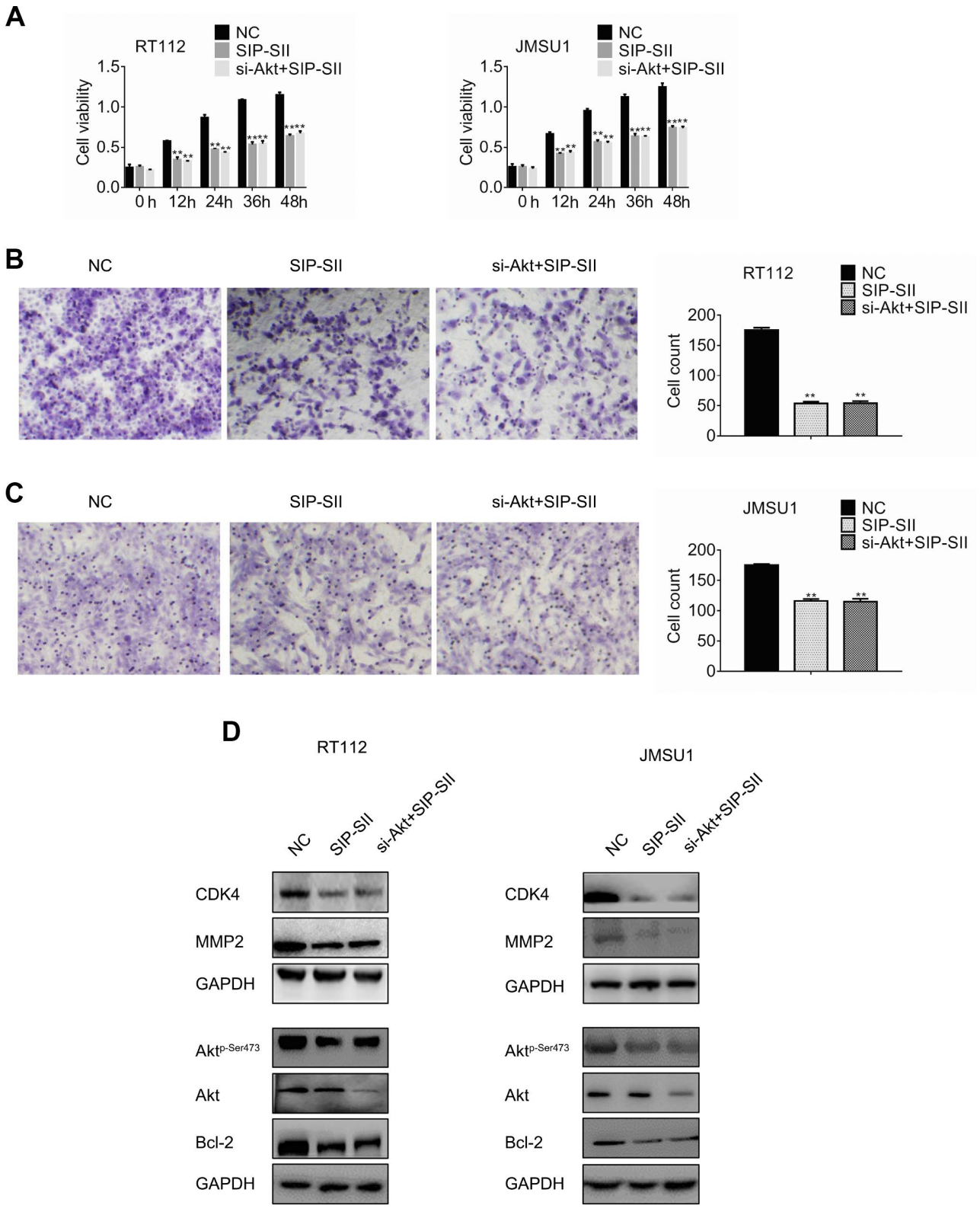

Figure 2. SIP-SII hampers proliferation and migration of bladder cancer cells in an Akt-dependent manner. (**A**) Cell viability (MTT) assay results for RT112 and JMSU1 cells treated with negative control siRNA (NC), 5.0 μM SIP-SII, or dual treatment with SIP-SII and Akt siRNA (si-Akt) for 24 h. Cell migration assay results for RT112 cells (**B**) and JMSU1 cells (**C**) treated with SIP-SII alone or in combination with si-Akt for 24 h. Representative images at 200x magnification. Data are mean ± SD (error bars) of three experiments performed in triplicate. **P < 0.01 vs. DMSO; n = 3. Western blot analyses of RT112 (**D**) and JMSU1 (**E**) cells treated with DMSO, SIP-SII, or the combination of SIP-SII and si-Akt for 24 h.

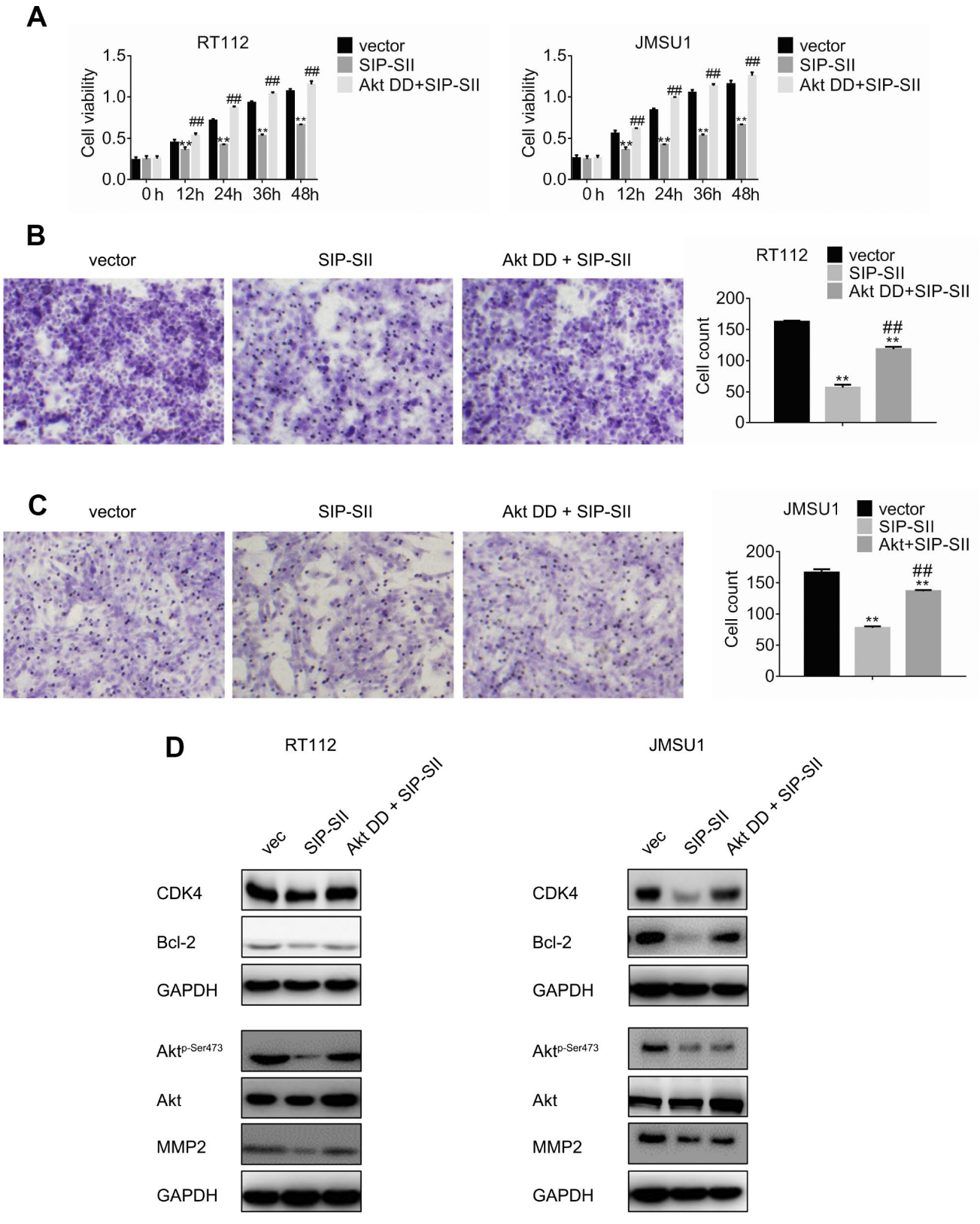

Figure 3. Overexpression of Akt DD abrogates SIP-SII inhibitory effects. (**A**) Cell viability assay results for RT112 and JMSU1 cells treated with the FLAG-HA empty vector and DMSO (control), 5.0 μM SIP-SII, or SIP-SII combined with Akt DD (PKB T308D S473D) for 24 h. Cell migration assay results for RT112 (**B**) and JMSU1 cells (**C**) treated with SIP-SII alone or in combination with Akt DD for 24 h. Representative images at 200x magnification. Data are mean ± SD (error bars) of three experiments performed in triplicate. **P < 0.01 vs. DMSO; n = 3. Western blot analyses in RT112 (**D**) and JMSU1 (**E**) cells treated with SIP-SII alone or in combination with Akt DD for 24 h.

Bcl-2, and MMP2 was restored in parallel with hyperactivation of Akt (Supplementary Figure 1C). These data strongly suggest that the inhibitory actions of SIP-SII on bladder cancer cells are dependent on Akt inhibition.

Dual treatment with SIP-SII and AZD4547 enhances the anticancer effects elicited by single inhibitors

Resistance to AZD4547 in RT112 and JMSU1 cells, carrying respectively a FGFR3-TACC3 translocation and FGFR1 amplification, is mediated by constitutively active PI3K/Akt signaling [7, 16]. To investigate the potential of SIP-SII in overcoming AZD4547 resistance, RT112 and JMSU1 cells were exposed to these inhibitors, either singly or in combination (Table 1), and the MTT assay was performed to determine compounded drug effects through estimation of the combination index (Table 2). The IC_{50} of combined drug exposure was lower than that measured for AZD4547 alone both in RT112 cells (0.43 μM vs 1.25 μM) and in JMSU1 cells (0.47 μM vs 1.28 μM). In turn, CI values were 0.7037 for RT112 and 0.7407 for JMSU1 (Table 2, indicating that the effects of the drug combination were synergistic. These results are exemplified in Figure 4A, showing enhanced inhibition of cell viability by combined treatment, compared with single exposure to SIP-SII (5 μM) or AZD4547 (100 nM).

Transwell assays were also performed to assess the effects of the combined inhibitors on cell migration. As shown in Figure 4B and 4C, migration declined by 70% after combination treatment, compared to the 50% reduction elicited by SIP-SII and AZD4547 separately. Furthermore, as sown in Figure 4D, cell cycle analysis indicated that the proportion of RT112 cells in G1 was significantly lower after combined drug treatment than after AZD4547 treatment alone (0.75% vs. 0.84% respectively; $P < 0.01$). Similar results were observed in JMSU1 cells (0.65% vs. 0.82% respectively; $P < 0.01$, Figure 4E). Additionally, the JC-1 assay was performed to evaluate apoptotic rates post-exposure to single or dual inhibitors. As shown in Figure 4F, the percentage of apoptotic RT112 cells increased from 0.69% in the AZD4547 group to 1.68% in the combination group ($p < 0.01$). Similar results were obtained in JMSU1 cells (0.93% vs. 1.84%, respectively; $P < 0.01$, Figure 4G). These results indicate that combination therapy decreased bladder cancer cell migration and promoted cell cycle arrest and apoptosis to a larger extent than AZD4547 monotherapy.

SIP-SII specifically targets Akt

The effects of combined SIP-SII and AZD4547 treatment on Akt activation and expression of downstream signaling molecules were explored through western blot. As shown in Figure 5A, the expression of phospho-Akt, CDK4, Bcl-2, and MMP2 in RT112 cells was downregulated to a greater by SIP-SII and AZD4547 combined, compared to AZD4547 alone. Similar results were obtained in JMSU1 cells. These results were validated by gel analysis (Supplementary Figure 1D), indicating that combination therapy might overcome AZD4547 resistance by blocking Akt-mediated pathways. To further explore SIP-SII specificity, the selective PI3K inhibitor BKM120 was used to inhibit AKT activation. RT112 cells were treated for 24 h with DMSO (vehicle), 5 μM SIP-SII, 100 nM AZD4547, or SIP-SII combined with both AZD4547 and 0.5 μM BKM120. Western blots results showed that phospho-AKT, CDK4, Bcl-2, and MMP2 decreased significantly, while total AKT showed little change in cells treated with the three inhibitors (Figure 5B). Addition of BKM120 did not further enhance the suppression of AKT phosphorylation elicited by SIP-SII, indicating specific inhibition of Akt signaling by SIP-SII. These findings were corroborated by gel analysis (Supplementary Figure 1E). In addition, the effects of the combined inhibitors on cell growth were evaluated through MTT assays. Figure 5C shows that the combination of BKM120 and AZD4547 enhanced growth inhibition compared to AZD4547 alone. In contrast, dual treatment with BKM120 and SIP-SII neither enhanced nor reduced the suppression induced by SIP-SII. On the other hand, migration assay results indicated that dual treatment with BKM120 and AZD4547 promoted a stronger inhibition than that elicited by AZD4547 alone, whereas the inhibition induced by combined BKM120 and SIP-SII exposure was similar to that produced by SIP-SII alone. These results further imply that SIP-SII inhibits bladder cancer cell proliferation and migration by targeting Akt.

Combination of SIP-SII and AZD4547 enhances growth inhibition of RT112 xenografts

To assess whether the SIP-SII and AZD4547 combinatorial regimen suppresses tumor growth in vivo, subcutaneous RT112 xenografts were generated in C57BL/6 mice. When tumors reached a mean volume of ~100 mm^3, mice were divided into four groups and treated respectively with saline, SIP-SII, AZD4547, or the combination of SIP-SII and AZD4547. As shown in Figure 6A, tumor growth was initially reduced by each inhibitor alone, but the effects diminished gradually over time. In contrast, sustained tumor regression was observed during combined SIP-SII and AZD4547 administration. In parallel with decreased tumor volumes, tumor weights in the drug combination group were significantly reduced compared to the control group (0.47 g vs. 1.7 g; $P < 0.01$) while those in the monotherapy groups showed a more modest reduction (0.84 g and

Table 1. IC_{50} values of SIP-SII and AZD4547 for cells treated with single inhibitor or dual inhibitors.

Cell line	Single inhibitor		Dual inhibitors	
	SIP-SII	AZD4547	SIP-SII	AZD4547
RT112	6.735	1.252	2.410	0.433
JMSU1	7.395	1.280	2.785	0.466

Notes: Bladder cancer cells were treated with single inhibitor or dual inhibitors as indicated. IC_{50} values (μM) were calculated using log vs. response - variable slop. Data are the mean of two independent experiments performed in triplicate. SIP-SII, Sulfated polysaccharide of *Sepiella maindroni* ink.

Table 2. Combination index (CI) at ED_{50} values of drug combination on two bladder cancer cell lines.

Cell line	SIP-SII	AZD4547	CI at ED50
RT112	6.735	1.252	0.7037
JMSU1	7.395	1.280	0.7407

Notes: Bladder cancer cells were treated with various drugs combination as indicated. CI values at 50% effective doses (ED_{50}) were calculated using Chou-Talalay method. Data are the mean of two independent experiments performed in triplicate. SIP-SII, Sulfated polysaccharide of *Sepiella Maindroni* ink.

0.86 g for SIP-SII and AZD4547, respectively; $P < 0.01$; Figure 6B). Body weights were not significantly altered by any treatment, suggesting that the interventions were well tolerated (Figure 6C).

After tumor excision, the expression of phospho-Akt was verified by immunohistochemistry. As shown in Figure 6D, phosphorylation of Akt decreased remarkably in the SIP-SII group and in the combined treatment group. Furthermore, western blots demonstrated a stronger decrease in the expression of CDK4, Bcl-2, and MMP2 in the combination group, compared to each single treatment (Figure 6E and Supplementary Figure 1F). Thus, results of in vivo experiments suggested that combination of SIP-SII and AZD4547 induced gradual and sustained tumor regression by concomitant inhibition of FGFR and Akt.

DISCUSSION

Akt hyperactivation is a common mechanism underlying resistance to FGFR inhibitors in cancers of the bladder with FGFR hyperactivation or overexpression. Our study suggests a potential novel strategy to overcome such resistance by showing that SIP-SII, a chemically sulfated polysaccharide isolated from the ink of the cuttlefish *Sepiella maindroni*, inhibits Akt activation and sensitizes bladder cancer cells to the anti-tumor actions of the FGFR inhibitor AZD4547.

Bladder carcinomas typically carry a large number of DNA mutations, surpassed only by lung cancers and melanoma [17]. Among the DNA alterations commonly found in tumors of the bladder, *PIK3CA*, *FGFR3*, and *ERBB2/3* mutations constitute promising targets for targeted therapies [2, 17]. Among the most relevant signaling pathways investigated in animal models of bladder cancer are the EGFR-RAS-MAPK [18], FGFR3-RAS-MAPK [19], VEGF-RAS-MAPK [20], PI3K-Akt-mTOR [21, 22], AR-PI3K/Akt [23], and STAT3-Survivin [24] pathways. Among those, receptor tyrosine kinases (EGFR, FGFR, and VEGFR) signaling through Ras-MAPK or Ras-PI3K-Akt axes are the most frequently hyperactive pathways implicated in bladder cancer progression [25–27]. Many compounds have been developed and are being tested in pre-clinical studies and clinical trials for bladder cancer. These include the FGFR inhibitors erdafitinib (approval), BGJ398 (Phase 1), and AZD4547 (Phase 1), the PI3K-beta inhibitor GSK2636771 (Phase 1), and the EGFR inhibitors erlotinib (Phase 2) and afatinib (Phase 2). However, common challenges to trial success include limited response rate, lack of treatment effect, and rapid occurrence of drug resistance, which reflect the large genetic heterogeneity of bladder cancer. About two-thirds of all non-muscle invasive bladder cancers carry activating *FGFR3* mutations [28] while more than 40% of muscle-invasive bladder cancers overexpress FGFR3 [29]. The frequency of activating *FGFR3* mutations and gene-fusion events (e.g. FGFR3-TACC3, FGFR3-BAIAP2L1, and FGFR3-JAKMIP1) provides a solid rationale for the success of erdafitinib, the first FGFR inhibitor approved by the FDA. However, rapid onset of erdafitinib resistance restrained its therapeutic success. Compared to more rare mutations in the *RAS* family, activating mutations of the PI3K-Akt axis appear in approximately 20% of bladder carcinomas, conferring resistance to FGFR inhibitors. Besides, mutational hyperactivation of *FGFR2*, overexpression of MET, and the *JHDM1D-BRAF* fusion [8, 9] have also been found to contribute to intrinsic and acquired resistance to FGFR inhibitors.

In this study we show that SIP-SII inhibits growth and migration of bladder cancer cells, while also potentiating

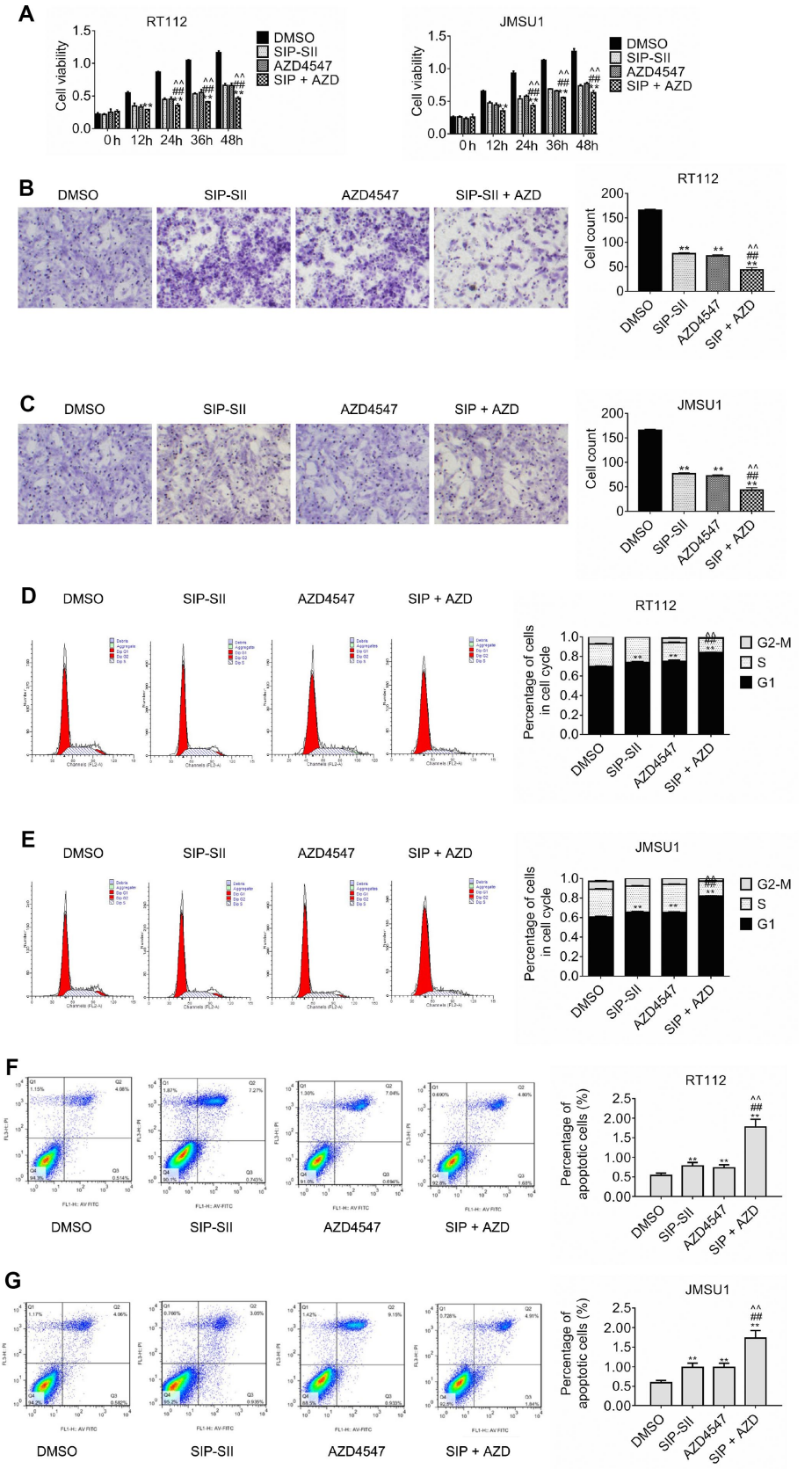

Figure 4. Inhibition of cell proliferation and migration by dual treatment with SIP-SII and AZD4547. (**A**) Results of cell viability assays in RT112 and JMSU1 cells cultured with DMSO, 5.0 μM SIP-SII, 100 nM AZD4547, or SIP-SII and AZD4547 combined. Transwell

migration assay results for RT112 (**B**) and JMSU1 (**C**) cells treated with DMSO, 5.0 μM SIP-SII, 100 nM AZD4547, or the combination of SIP-SII and AZD4547 for 24 h. Representative images at 200x magnification. Cell cycle analyses of RT112 (**D**) and JMSU1 (**E**) cells treated with DMSO, 5.0 μM SIP-SII, 100 nM AZD4547, or dual treatment with SIP-SII and AZD4547. Flow cytometry was performed 24 h post-treatment in PI-stained cells. JC-1 apoptosis assay results in RT112 (**F**) and JMSU1 (**G**) cells treated (24 h) with DMSO, 5.0 μM SIP-SII, 100 nM AZD4547, or the combination of SIP-SII and AZD4547. Data are mean ± SD (error bars) of three individual experiments. **P < 0.01 vs. DMSO; ##P < 0.01 vs. SIP-SII; ^^P < 0.01 vs. AZD4547; n = 3.

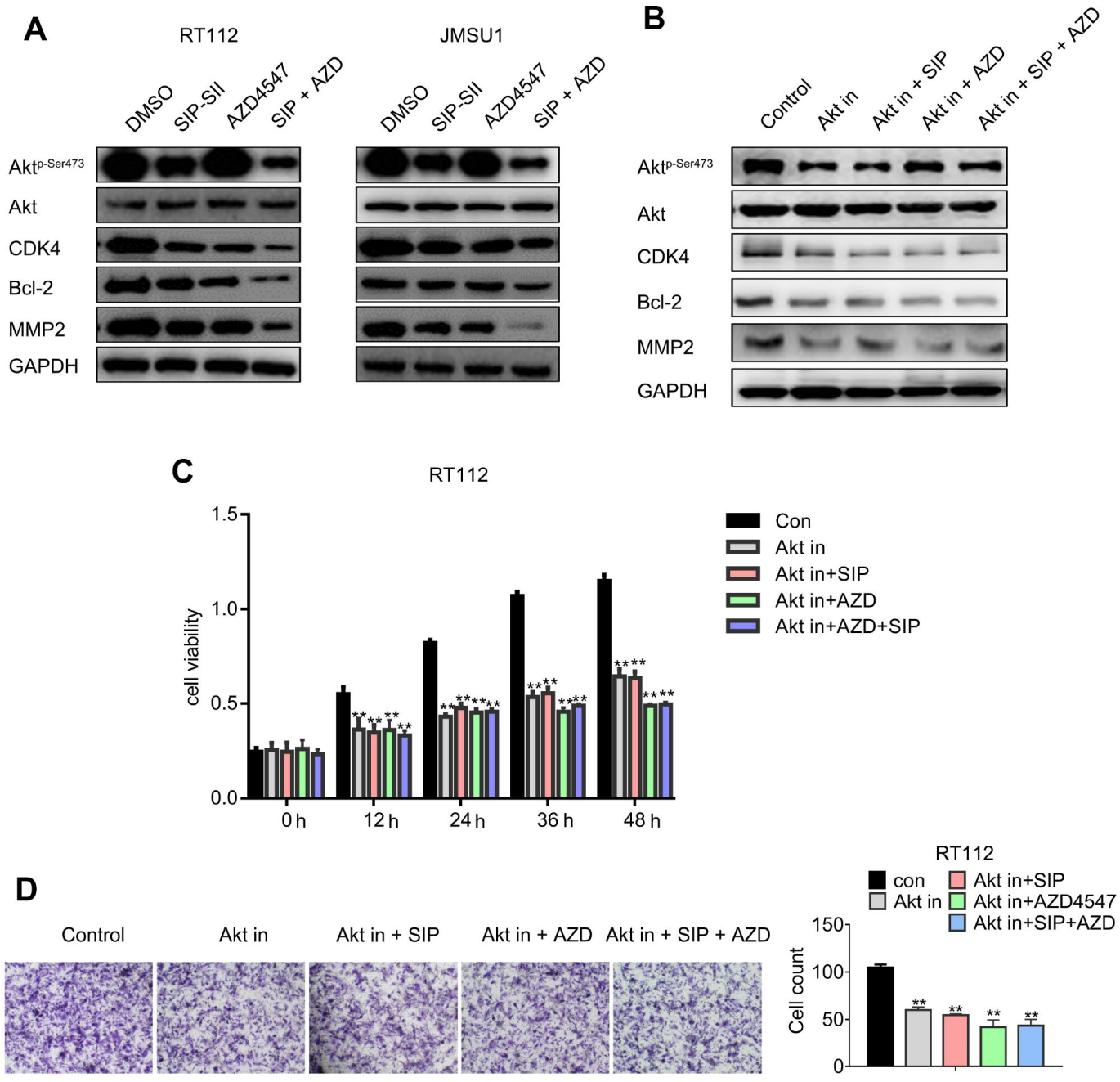

Figure 5. Dual treatment with SIP-SII and AZD4547 potentiates the inhibition of Akt and downstream effectors. (**A**) Western blot analysis of RT112 and JMSU1 cells exposed (24 h) to DMSO, 5.0 μM SIP-SII, 100 nM AZD4547, or SIP-SII combined with AZD4547. (**B**) Western blot analysis of RT112 and JMSU1 cells treated for 24 h with DMSO, 5.0 μM SIP-SII, 100 nM AZD4547, or SIP-SII combined with AZD4547 in the presence of 0.5 μM BKM120. Akt in, Akt inhibitor BKM120. ** vs. Con, ## vs. AKT IN, ^^ vs. AKT IN+SIP, $$ vs. AKT IN+AZD. **, ##, ^^ and $$ indicated P < 0.01, n=3. (**C**) Cell viability assay results. (**D**) Transwell migration assay results. Representative images at 200x magnification. Data are mean ± SD (error bars) of three individual experiments. **P < 0.01 vs. control; n = 3.

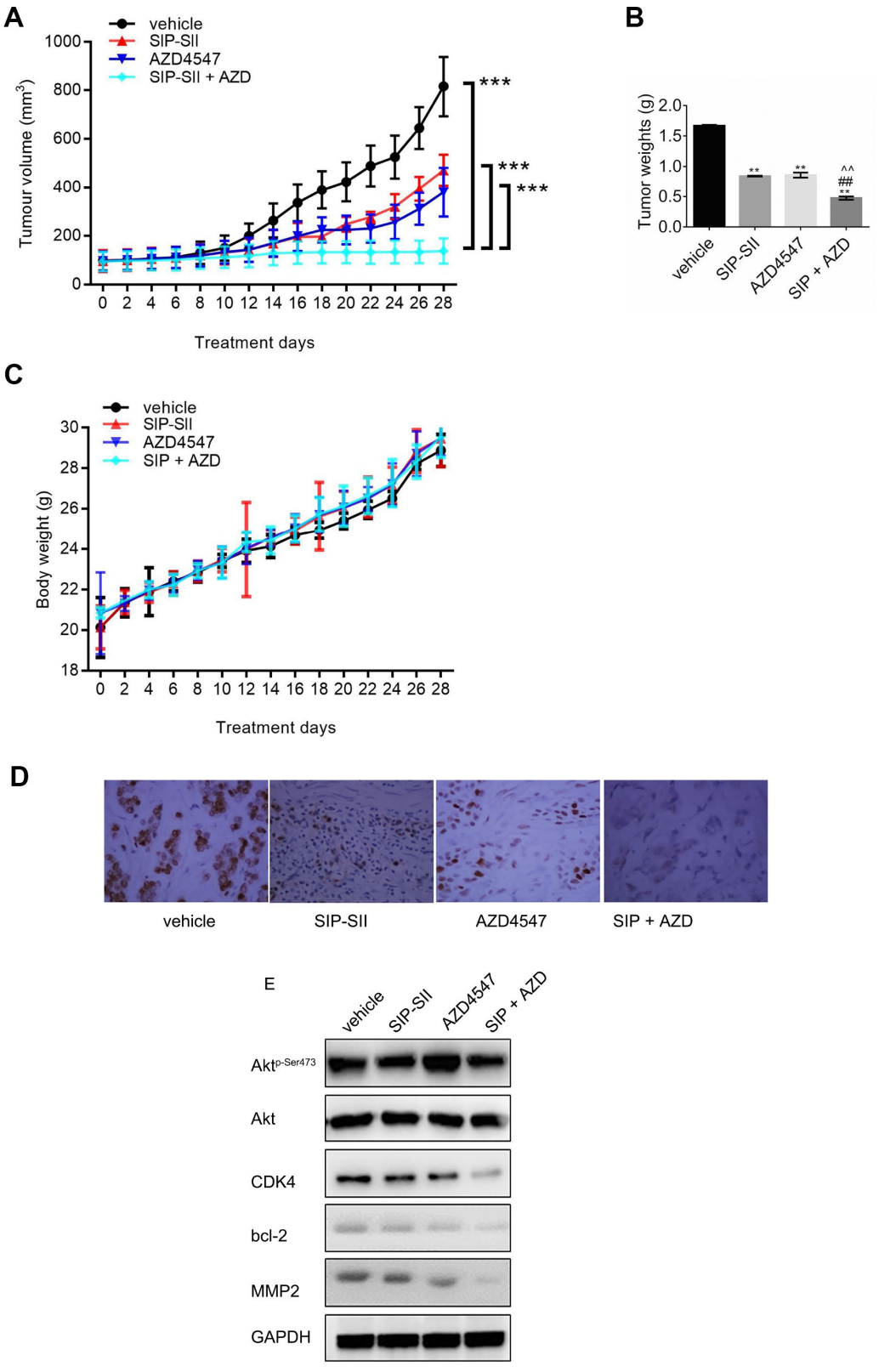

Figure 6. Combination of SIP-SII and AZD4547 enhances growth suppression of RT112 xenografts. Nude mice were randomly divided into four experimental groups after subcutaneous injection of RT112 cells. (**A**) Tumor volume measurements. (**B**) Tumor weight measurements after euthanasia on day 28 post-treatment initiation. (**C**) Body weight measurements. ***P < 0.001 vs. DMSO control; n = 3 per group. (**D**) Immunohistochemical staining of phospho-Akt in excised tumors (vehicle, SIP-SII, AZD4547, and combination therapy). Representative images at 100x magnification. (**E**) Western blot analysis of tumor samples.

the inhibitory effects of the small molecule pan-FGFR inhibitor AZD4547. SIP-SII exhibits broad anti-tumor effects. For instance, it was shown to repress lung metastasis of B16F10 melanoma xenografts in mice via inhibition of MMP2 [13], and to inhibit EGFR-Ras-MEK-MMP2 and EGFR-PI3K-MMP2 pathways in an EGF-dependent manner in KB cells [14]. Nevertheless, the effects of SIP-SII on bladder cancer cells with active PI3K-Akt signaling had not been explored. We demonstrated that SIP-SII exposure reduced the expression of MMP2, CDK4, and Bcl-2, hinting at potential mechanisms underlying impaired cell migration, promotion of cell cycle arrest, and increased apoptosis following AKT inactivation. The fact that neither siRNA-mediated Akt silencing nor co-treatment with the PI3K inhibitor BKM120 further increased the inhibitory effects of SIP-SII, while forced expression of a constitutively active Akt mutant reversed such effects, proves that SIP-SII effectively inactivates Akt at low micromolar doses in bladder cancer cells.

Our xenograft model expanded the findings obtained in vitro, demonstrating that the combination of SIP-SII and AZD4547 overcome AZD4547 resistance and significantly reduced tumor growth compared to each monotherapy regimen, without patent adverse effects. Therefore, in future studies the selectivity, pharmacological dynamics, and maximum tolerated dose of SIP-SII should be investigated in detail. In addition, experiments in bladder cancer cells harboring *FGFR3* fusions and activating PI3K/Akt mutations should also be conducted to explore the efficacy of SIP-SII in combination with FGFR inhibitors under more restrictive mutational landscapes.

MATERIALS AND METHODS

Cell lines, transfection reagents, drugs, and antibodies

Human bladder cancer RT112 (ACC-418) and JMSU1 (ACC-505) cells were obtained from the Leibniz Institute DSMZ - German Collection of Microorganisms and Cell Cultures GmbH (Inhoffenstraße, Braunschweig, Germany). RT112 cells carry a FGFR3-TACC3 translocation, while JMSU1 cells harbor FGFR1 amplification [7]. Cells were cultured in Dulbecco's Modified Eagle Medium (DMEM) supplemented with 10% fetal bovine serum (FBS, Thermo Fisher Scientific Inc., Waltham, MA, USA) at 37°C in a humid incubator containing 5% CO_2 and 95% air.

Control siRNA (sc-37007) and Akt1/2 siRNA (sc-43609) were obtained from Santa Cruz Biotechnology, Inc. (Dallas, Texas, USA). The selective FGFR inhibitor AZD4547 (S2801) was purchased from Selleckchem (Houston, TX, USA). SIP-SII was prepared following the protocol described previously [11]. HA PKB T308D S473D pcDNA3 (Akt DD) was a gift from Jim Woodgett (Addgene plasmid #14751; http://n2t.net/addgene:14751; RRID: Addgene_14751) [30]. Empty vector FLAG-HA-pcDNA3.1- was a gift from Adam Antebi (Addgene plasmid #52535; http://n2t.net/addgene:52535; RRID: Addgene_52535) [31]. The selective PI3K inhibitor BKM120 (S2247) was purchased from Selleck Chemicals Inc. (Shanghai, China). Antibodies against p-Akt1/2/3 (sc-514032), Akt1/2/3 (sc-81434), Cdk4 (sc-70832), Bcl-2 (sc-509), MMP-2 (sc-13594), and GAPDH (sc-47724) were obtained from Santa Cruz Biotechnology, Inc. (Shanghai, China).

Cell viability analysis

RT112 or JMSU1 cells were seeded in 96-well plates ($5x10^3$ cells/well) and allowed to attach overnight. Next, cells were treated with SIP-SII, AZD4547, or the combination of SIP-SII and AZD4547 for 12, 24, 36, 48, or 72 h, after which 20 μL of a 5 mg/mL stock of methylthiazolyldiphenyl-tetrazolium bromide (MTT, 298-93-1, Sigma-Aldrich Inc., St. Louis, MO, USA) was added to the medium. Cells were further incubated at 37 °C for 4 h, centrifuged, and the pellet was dissolved in 150 μL of DMSO. Absorbance was measured at 570 nm on a microplate reader (Bio-Rad 680 XR, Hercules, CA, USA). The combination index (CI) of SIP-SII and AZD4547 was calculated using the Chou-Talalay method, where $CI < 1$, $CI = 1$, and $CI > 1$ indicate synergism, additive effect, and antagonism in drug combinations, respectively [32].

Transwell migration assay

The transwell migration assay was performed as reported before, using membranes with 8 μm pore size [33]. In brief, $3x10^4$ bladder cancer cells suspended in 50 μL of serum-free DMEM were seeded in the upper chambers and treated with test compounds. The lower wells were filled with 600 μL of DMEM containing 10% FBS. After a 24 h incubation, cells on the upper surface of the membrane were removed with cotton swabs and cells that migrated to the lower surface were fixed, stained, and counted under an inverted microscope. Five random fields in each group were recorded.

Western blotting

Attached cells were washed twice with ice-cold PBS and then lysed with lysis buffer for 30 min on ice. Total protein content (for cell and tissue samples) was determined using a BCA protein assay kit (ab102536, Abcam, Cambridge, UK). Equal amounts of proteins were resolved by 10% SDS-PAGE and transferred

onto polyvinylidene fluoride (PVDF) membranes. The membranes were blocked with 5% skim milk in TBS-T for 1 h and incubated with specific primary antibodies (1:1000) at 4 °C with gentle shaking overnight. Membranes were washed three times with TBS-T, reacted with secondary antibodies conjugated to HRP (1:2000; ab205719 and ab205718, Abcam, Cambridge, UK), and antibody:protein complexes detected by enhanced chemiluminescence (Pierce; Thermo Fisher Scientific, Inc.). Data obtained from three independent experiments were analyzed with ImageJ software (v 1.52p).

Cell cycle analysis

Cell cycle distribution analysis was performed using the Propidium Iodide (PI) Flow Cytometry Kit (ab139418, Abcam, Cambridge, UK) following the manufacturer's protocol. Untreated cells were used as control. Cells were prepared at a density of $1x10^4$ per well in 6 well plates and exposed to test reagents for 24 h at 37ºC. After harvesting and preparation of single-cell suspensions, cells were fixed, stained with PI, and analyzed on a FACSCalibur cytometer (BD Biosciences, San Jose, CA, US). Cell cycle distribution analysis was performed on three separate experiments using BD CellQuest™ Pro Analysis software (BD Biosciences, San Jose, CA, US).

Apoptosis analysis

For apoptosis analysis, cells ($2x10^5$) were seeded in 6-well plates and allowed to attach overnight. Experimental treatments were applied, and cells were then harvested and stained with the mitochondrial membrane potential reporter JC-1 (ab141387, Abcam, Cambridge, UK). JC-1 fluorescence was assessed by flow cytometry in three individual experiments.

Xenograft model

Animal experiments were approved by the Institutional Animal Care and Use Committee of Shengjing Hospital of China Medical University (Shenyang, China). Nude mice (male, 18–22 g) were obtained from the Experimental Animal Centre of Shengjing Hospital of China Medical University. RT112 cells ($5×10^6$ in 0.2 mL of saline) were subcutaneously injected into the right axilla of mice. When tumor volumes reached ~100 mm^3 mice were randomly divided into four groups (n = 3 per group): control (saline, vehicle), SIP-SII (30 mg/kg/d), AZD4547 (30 mg/kg/d), and combination of SIP-SII and AZD4547 (SIP + AZD). All drugs were administered by intraperitoneal injection (0.2 mL) every day for 28 days. Tumor volumes and body weights were documented every other day. Mice were euthanized by cervical dislocation under isoflurane anaesthesia 24 h after the last drug injection.

Immunohistochemistry

Tumors were harvested, fixed with 10% neutral buffered formalin, and embedded in paraffin. Representative tumor sections were incubated with a p-Akt-Ser473 antibody (sc-514032, Santa Cruz Biotechnology, Inc., Dallas, Texas, US) and immunoreactivity detected using the Ultra-Sensitive™ SAP IHC staining kit (KIT-7710, Maixin Biotech., Fuzhou, China).

Statistical analysis

Data were analyzed using GraphPad Prism 7.00 (GraphPad Software, San Diego, CA, USA) and are expressed as the mean ± standard deviation (SD). Multiple comparisons were performed using two-way analysis of variance (ANOVA) and Tukey's multiple comparisons test. Multiple comparisons of tumor weights were performed by one-way ANOVA and Tukey's multiple comparisons test. $P < 0.05$ was considered statistically significant.

Abbreviations

RTK: receptor tyrosine kinase; EGFR: epidermal growth factor receptor; FGFR: fibroblast growth factor receptor; PI3K: phosphatidylinositol-3-kinase; AKT: protein kinase B; mTOR: mammalian target of rapamycin; MAPK: mitogen-activated protein kinase; ERK: extracellular-signal-regulated kinase; RAS: RAS type GTPase family; JAK: tyrosine-protein kinase JAK; STAT: signal transducer and activator of transcription; MET: MET protooncogene, receptor tyrosine kinase; Bcl-2: apoptosis regulator Bcl-2; CDK4: cyclin-dependent kinase 4; MMP2: matrix metallopeptidase 2; SIP-SII: sulfated polysaccharide of *Sepiella maindroni* ink.

AUTHOR CONTRIBUTIONS

LS wrote the main manuscript. LS and WL performed the experiments, designed the research, and performed data analysis. YZ contributed to manuscript revisions. All authors reviewed and approved the final manuscript.

CONFLICTS OF INTEREST

The authors declare that there are no conflicts of interest concerning this article.

REFERENCES

1. Bray F, Ferlay J, Soerjomataram I, Siegel RL, Torre LA, Jemal A. Global cancer statistics 2018: GLOBOCAN estimates of incidence and mortality worldwide for 36 cancers in 185 countries. CA Cancer J Clin. 2018;

68:394–424.
https://doi.org/10.3322/caac.21492
PMID:30207593

2. Cancer Genome Atlas Research Network. Comprehensive molecular characterization of urothelial bladder carcinoma. Nature. 2014; 507:315–22.
https://doi.org/10.1038/nature12965 PMID:24476821

3. Morales-Barrera R, Suárez C, de Castro AM, Racca F, Valverde C, Maldonado X, Bastaros JM, Morote J, Carles J. Targeting fibroblast growth factor receptors and immune checkpoint inhibitors for the treatment of advanced bladder cancer: New direction and New Hope. Cancer Treat Rev. 2016; 50:208–16.
https://doi.org/10.1016/j.ctrv.2016.09.018
PMID:27743530

4. Saka H, Kitagawa C, Kogure Y, Takahashi Y, Fujikawa K, Sagawa T, Iwasa S, Takahashi N, Fukao T, Tchinou C, Landers D, Yamada Y. Safety, tolerability and pharmacokinetics of the fibroblast growth factor receptor inhibitor AZD4547 in Japanese patients with advanced solid tumours: a Phase I study. Invest New Drugs. 2017; 35:451–62.
https://doi.org/10.1007/s10637-016-0416-x
PMID:28070720

5. Bachir BG, Souhami L, Mansure JJ, Cury F, Vanhuyse M, Brimo F, Aprikian AG, Tanguay S, Sturgeon J, Kassouf W, Phase I. Phase I Clinical Trial of Everolimus Combined with Trimodality Therapy in Patients with Muscle-Invasive Bladder Cancer. Bladder Cancer. 2017; 3:105–12.
https://doi.org/10.3233/BLC-160090
PMID:28516155

6. Schmidt B, Wei L, DePeralta DK, Hoshida Y, Tan PS, Sun X, Sventek JP, Lanuti M, Tanabe KK, Fuchs BC. Molecular subclasses of hepatocellular carcinoma predict sensitivity to fibroblast growth factor receptor inhibition. Int J Cancer. 2016; 138:1494–505.
https://doi.org/10.1002/ijc.29893
PMID:26481559

7. Wang L, Šuštić T, Leite de Oliveira R, Lieftink C, Halonen P, van de Ven M, Beijersbergen RL, van den Heuvel MM, Bernards R, van der Heijden MS. A Functional Genetic Screen Identifies the Phosphoinositide 3-kinase Pathway as a Determinant of Resistance to Fibroblast Growth Factor Receptor Inhibitors in FGFR Mutant Urothelial Cell Carcinoma. Eur Urol. 2017; 71:858–62.
https://doi.org/10.1016/j.eururo.2017.01.021
PMID:28108151

8. Kas SM, de Ruiter JR, Schipper K, Schut E, Bombardelli L, Wientjens E, Drenth AP, de Korte-Grimmerink R, Mahakena S, Phillips C, Smith PD, Klarenbeek S, van de Wetering K, et al. Transcriptomics and Transposon Mutagenesis Identify Multiple Mechanisms of Resistance to the FGFR Inhibitor AZD4547. Cancer Res. 2018; 78:5668–79.
https://doi.org/10.1158/0008-5472.CAN-18-0757
PMID:30115694

9. Sase H, Nakanishi Y, Aida S, Horiguchi-Takei K, Akiyama N, Fujii T, Sakata K, Mio T, Aoki M, Ishii N. Acquired JHDM1D-BRAF Fusion Confers Resistance to FGFR Inhibition in *FGFR2*-Amplified Gastric Cancer. Mol Cancer Ther. 2018; 17:2217–25.
https://doi.org/10.1158/1535-7163.MCT-17-1022
PMID:30045926

10. Chowdhury VJ, Oscier DG, Mufti GJ, Hamblin TJ. Hairy cell leukaemia and Legionnaires' disease. Br J Dis Chest. 1985; 79:393–95.
https://doi.org/10.1016/0007-0971(85)90075-0
PMID:4052311

11. Wang S, Cheng Y, Wang F, Sun L, Liu C, Chen G, Li Y, Ward SG, Qu X. Inhibition activity of sulfated polysaccharide of Sepiella maindroni ink on matrix metalloproteinase (MMP)-2. Biomed Pharmacother. 2008; 62:297–302.
https://doi.org/10.1016/j.biopha.2008.01.018
PMID:18406565

12. Soliman AM, Fahmy SR, El-Abied SA. Anti-neoplastic activities of Sepia officinalis ink and Coelatura aegyptiaca extracts against Ehrlich ascites carcinoma in Swiss albino mice. Int J Clin Exp Pathol. 2015; 8:3543–55. PMID:26097537

13. Zong A, Zhao T, Zhang Y, Song X, Shi Y, Cao H, Liu C, Cheng Y, Qu X, Cao J, Wang F. Anti-metastatic and anti-angiogenic activities of sulfated polysaccharide of Sepiella maindroni ink. Carbohydr Polym. 2013; 91:403–09.
https://doi.org/10.1016/j.carbpol.2012.08.050
PMID:23044150

14. Jiang W, Tian W, Ijaz M, Wang F. Inhibition of EGF-induced migration and invasion by sulfated polysaccharide of Sepiella maindroni ink via the suppression of EGFR/Akt/p38 MAPK/MMP-2 signaling pathway in KB cells. Biomed Pharmacother. 2017; 95:95–102.
https://doi.org/10.1016/j.biopha.2017.08.050
PMID:28830011

15. Jiang W, Cheng Y, Zhao N, Li L, Shi Y, Zong A, Wang F. Sulfated polysaccharide of Sepiella maindroni ink inhibits the migration, invasion and matrix metalloproteinase-2 expression through suppressing EGFR-mediated p38/MAPK and PI3K/Akt/mTOR signaling pathways in SKOV-3 cells. Int J Biol Macromol. 2018; 107:349–362.
https://doi.org/10.1016/j.ijbiomac.2017.08.178
PMID:28870748

16. Gust KM, McConkey DJ, Awrey S, Hegarty PK, Qing J, Bondaruk J, Ashkenazi A, Czerniak B, Dinney CP, Black PC. Fibroblast growth factor receptor 3 is a rational therapeutic target in bladder cancer. Mol Cancer Ther. 2013; 12:1245–54. https://doi.org/10.1158/1535-7163.MCT-12-1150 PMID:23657946

17. Rentsch CA, Müller DC, Ruiz C, Bubendorf L. Comprehensive Molecular Characterization of Urothelial Bladder Carcinoma: A Step Closer to Clinical Translation? Eur Urol. 2017; 72:960–61. https://doi.org/10.1016/j.eururo.2017.06.022 PMID:28688612

18. Rebouissou S, Bernard-Pierrot I, de Reyniès A, Lepage ML, Krucker C, Chapeaublanc E, Hérault A, Kamoun A, Caillault A, Letouzé E, Elarouci N, Neuzillet Y, Denoux Y, et al. EGFR as a potential therapeutic target for a subset of muscle-invasive bladder cancers presenting a basal-like phenotype. Sci Transl Med. 2014; 6:244ra91. https://doi.org/10.1126/scitranslmed.3008970 PMID:25009231

19. Wu YM, Su F, Kalyana-Sundaram S, Khazanov N, Ateeq B, Cao X, Lonigro RJ, Vats P, Wang R, Lin SF, Cheng AJ, Kunju LP, Siddiqui J, et al. Identification of targetable FGFR gene fusions in diverse cancers. Cancer Discov. 2013; 3:636–47. https://doi.org/10.1158/2159-8290.CD-13-0050 PMID:23558953

20. Wang F, Li HM, Wang HP, Ma JL, Chen XF, Wei F, Yi MY, Huang Q. siRNA-mediated knockdown of VEGF-A, VEGF-C and VEGFR-3 suppresses the growth and metastasis of mouse bladder carcinoma in vivo. Exp Ther Med. 2010; 1:899–904. https://doi.org/10.3892/etm.2010.113 PMID:22993616

21. Seront E, Pinto A, Bouzin C, Bertrand L, Machiels JP, Feron O. PTEN deficiency is associated with reduced sensitivity to mTOR inhibitor in human bladder cancer through the unhampered feedback loop driving PI3K/Akt activation. Br J Cancer. 2013; 109:1586–92. https://doi.org/10.1038/bjc.2013.505 PMID:23989949

22. Zhou H, Huang HY, Shapiro E, Lepor H, Huang WC, Mohammadi M, Mohr I, Tang MS, Huang C, Wu XR. Urothelial tumor initiation requires deregulation of multiple signaling pathways: implications in target-based therapies. Carcinogenesis. 2012; 33:770–80. https://doi.org/10.1093/carcin/bgs025 PMID:22287562

23. Shiota M, Takeuchi A, Yokomizo A, Kashiwagi E, Tatsugami K, Kuroiwa K, Naito S. Androgen receptor signaling regulates cell growth and vulnerability to doxorubicin in bladder cancer. J Urol. 2012; 188:276–86. https://doi.org/10.1016/j.juro.2012.02.2554 PMID:22608749

24. Zhang B, Lu Z, Hou Y, Hu J, Wang C. The effects of STAT3 and Survivin silencing on the growth of human bladder carcinoma cells. Tumour Biol. 2014; 35:5401–07. https://doi.org/10.1007/s13277-014-1704-8 PMID:24519067

25. van Kessel KE, Zuiverloon TC, Alberts AR, Boormans JL, Zwarthoff EC. Targeted therapies in bladder cancer: an overview of in vivo research. Nat Rev Urol. 2015; 12:681–94. https://doi.org/10.1038/nrurol.2015.231 PMID:26390971

26. Mooso BA, Vinall RL, Mudryj M, Yap SA, deVere White RW, Ghosh PM. The role of EGFR family inhibitors in muscle invasive bladder cancer: a review of clinical data and molecular evidence. J Urol. 2015; 193:19–29. https://doi.org/10.1016/j.juro.2014.07.121 PMID:25158272

27. Robertson AG, Kim J, Al-Ahmadie H, Bellmunt J, Guo G, Cherniack AD, Hinoue T, Laird PW, Hoadley KA, Akbani R, Castro MAA, Gibb EA, Kanchi RS, et al. Comprehensive Molecular Characterization of Muscle-Invasive Bladder Cancer. Cell. 2017; 171:540–556.e525. https://doi.org/10.1016/j.cell.2017.09.007 PMID:28988769

28. van Rhijn BW, Zuiverloon TC, Vis AN, Radvanyi F, van Leenders GJ, Ooms BC, Kirkels WJ, Lockwood GA, Boevé ER, Jöbsis AC, Zwarthoff EC, van der Kwast TH. Molecular grade (FGFR3/MIB-1) and EORTC risk scores are predictive in primary non-muscle-invasive bladder cancer. Eur Urol. 2010; 58:433–41. https://doi.org/10.1016/j.eururo.2010.05.043 PMID:20646825

29. Tomlinson DC, Baldo O, Harnden P, Knowles MA. FGFR3 protein expression and its relationship to mutation status and prognostic variables in bladder cancer. J Pathol. 2007; 213:91–98. https://doi.org/10.1002/path.2207 PMID:17668422

30. Scheid MP, Marignani PA, Woodgett JR. Multiple phosphoinositide 3-kinase-dependent steps in activation of protein kinase B. Mol Cell Biol. 2002; 22:6247–60. https://doi.org/10.1128/MCB.22.17.6247-6260.2002 PMID:12167717

31. Horn M, Geisen C, Cermak L, Becker B, Nakamura S, Klein C, Pagano M, Antebi A. DRE-1/FBXO11-dependent degradation of BLMP-1/BLIMP-1 governs C. elegans developmental timing and maturation. Dev Cell. 2014; 28:697–710.

https://doi.org/10.1016/j.devcel.2014.01.028 PMID:24613396

32. Chou TC. Drug combination studies and their synergy quantification using the Chou-Talalay method. Cancer Res. 2010; 70:440–46. https://doi.org/10.1158/0008-5472.CAN-09-1947 PMID:20068163

33. Justus CR, Leffler N, Ruiz-Echevarria M, Yang LV. In vitro cell migration and invasion assays. J Vis Exp. 2014; 88: 51046. https://doi.org/10.3791/51046 PMID:24962652

SUPPLEMENTARY MATERIAL

Supplementary Figure

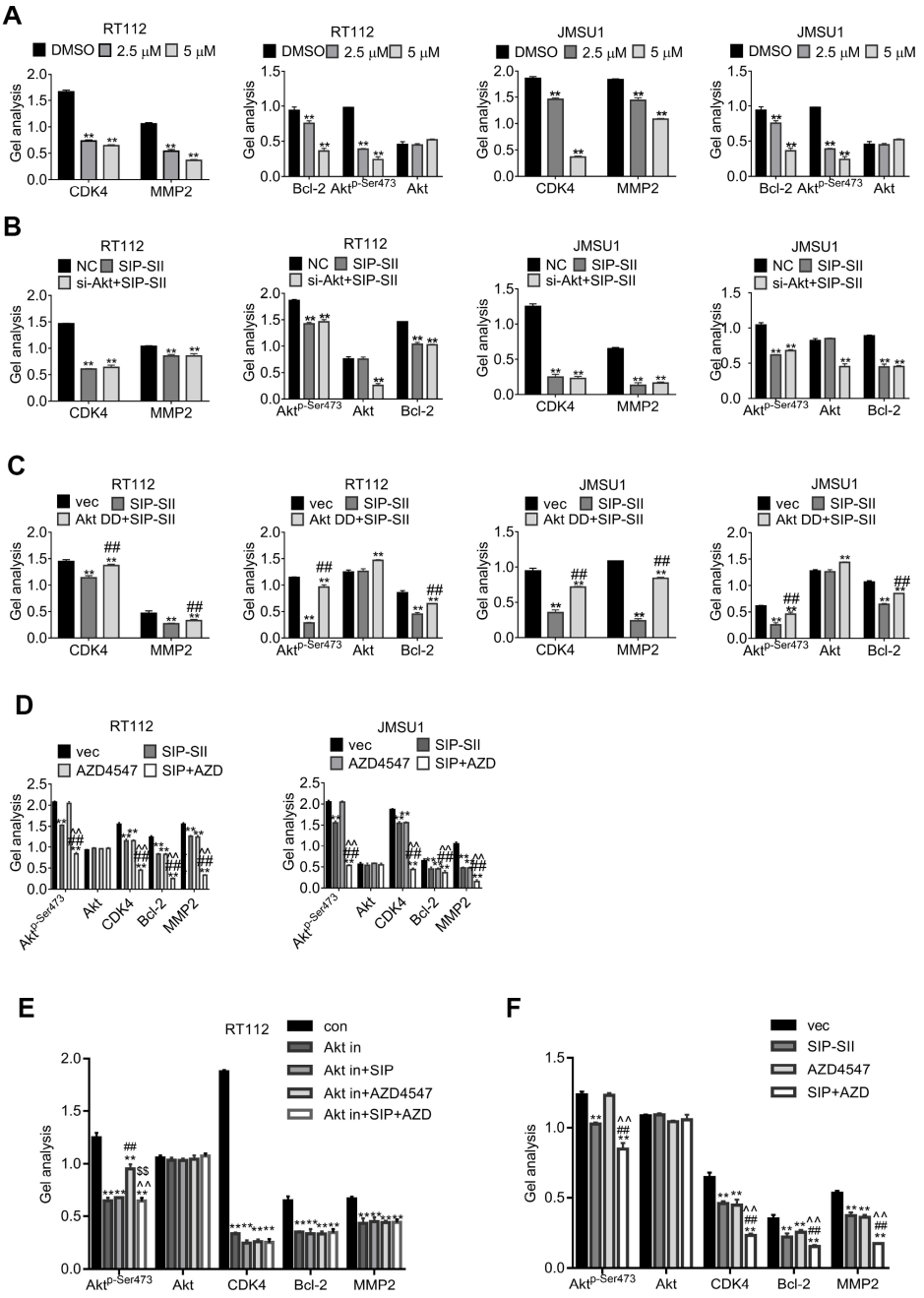

Supplementary Figure 1. Gel analysis of repeated western blots. (**A**) RT112 and JMSU1 cells were treated with DMSO, or 2.5 μM (RT112) and 5.0 μM SIP-SII (JMSU1) for 24 h. (**B**) RT112 and JMSU1 cells were treated with DMSO, SIP-SII, or the combination of SIP-SII and si-Akt for 24 h. (**C**) RT112 and JMSU1 cells were treated with DMSO, SIP-SII, or the combination of SIP-SII and Akt DD for 24 h. (**D**) RT112 and JMSU1 cells were treated with DMSO, 5.0 μM SIP-SII, 100 nM AZD4547, or SIP-SII combined with AZD4547. (**E**) RT112 and JMSU1 cells were treated with DMSO, 5.0 μM SIP-SII, 100 nM AZD4547, or SIP-SII combined with AZD4547 in the presence of 0.5 μM BKM120. In all cases, analyses were carried out 24 h post-treatment. ** vs. Con, ## vs. AKT IN, ^^ vs. AKT IN+SIP, $$ vs. AKT IN+AZD. **, ##, ^^ and $$ indicated $p < 0.01$, n=3. (**F**) Western blot analysis of tumor xenograft samples from mice treated with saline, SIP-SII, AZD4547, or the combination of SIP-SII and AZD4547. Data obtained from three individual experiments were analyzed by ImageJ. ** vs. Control; ## vs. SIP-SII; ^^ vs. AZD4547. **, ##, and ^^ indicated $P < 0.01$, n=3.